Journal of The Electrochemical Society, **158** (4) A390-A395 (2011)
0013-4651/2011/158(4)/A390/6/$28.00 © The Electrochemical Society

Li Diffusivity and Phase Change in $LiFe_{0.5}Mn_{0.5}PO_4$: A Comparative Study using Galvanostatic Intermittent Titration and Cyclic Voltammetry

A. M. Hashambhoy[a,*] and J. F. Whitacre[a,b,,z]**

[a]*Department of Materials Science and Engineering and* [b] *Department of Engineering and Public Policy, Carnegie Mellon University, Pittsburgh, Pennsylvania 15213, USA*

Lithium transport and phase evolution in the $LiFe_{0.5}Mn_{0.5}PO_4$ system was examined using both cyclic voltammetry and galvanostatic intermittent titration. Hydrothermal or sol–gel processing was used to synthesize $LiFe_{0.5}Mn_{0.5}PO_4$, $LiFePO_4$, and $LiMnPO_4$, and electrodes made with $LiFe_{0.5}Mn_{0.5}PO_4$ or a 1:1 mass ratio of $LiFePO_4$ and $LiMnPO_4$ were produced and studied. Cyclic voltammetry was used to distinguish single- and dual-phase redox reaction regimes and also accurately measure ionic diffusivity in the dual redox couple $LiFe_{0.5}Mn_{0.5}PO_4$ system. Ionic diffusivity values extracted from galvanostatic intermittent titration data were compared to those determined via cyclic voltammetry.These results are discussed in the context of theories that explain phase transitions and diffusion in this class of materials.
© 2011 The Electrochemical Society. [DOI: 10.1149/1.3545972] All rights reserved.

Manuscript submitted September 10, 2010; revised manuscript received January 3, 2011. Published February 22, 2011.

Lithium transition metal phosphates are among the frontrunners in cathode materials for hybrid electric vehicle batteries of the near future. Specifically, $LiFePO_4$ has demonstrated structural stability, a high potential (3.5 V vs Li/Li^+), a high theoretical specific capacity (~170 mAh/g), and the ability to be engineered to support a high C-rate cycling and is made up of environmentally benign constituents,[1–7] making it a safer, more robust alternative to $LiCoO_2$. Early investigation into the manganese analog of this system, $LiMnPO_4$ demonstrated a higher potential (4.1 V vs Li/Li^+); however, its limited rate capability made it impractical for commercial applications. A more recent study by Martha et al.[8] has illustrated improved performance of $LiMnPO_4$ reaching specific capacity of 140 mAh/g at a C/10 rate with a relatively low capacity fade, which is a promising step toward practical implementation, though much is yet to be understood about this materials system.

Padhi et al.[9] and Yamada et al.[10–12] pioneered interests in $LiFe_{1-y}Mn_yPO_4$, showing that the substitution of some percentage of octahedral 4c sites of $LiFePO_4$ with Mn, made it possible to access the higher potential of Mn as well as reach near theoretical capacity. This ability to increase the energy density of $LiFePO_4$ by substituting a portion of Fe sites with Mn has been the driving force for extensive research on $LiFe_{1-y}Mn_yPO_4$. By understanding how the dual transition metal system operates, it may be possible to create a material with a higher energy density than $LiFePO_4$ with no significant increase in cost, at rates acceptable for commercial applications.

There is, concurrently, a lack of understanding of diffusion versus phase change in these dual transition metal phosphates, which has motivated this study. The shrinking core-shell model, once widely accepted for olivine structures, has more recently been countered by the domino-cascade model,[13] an alternative theory, which, with the support of high resolution electron microscopy data, describes the relationship between lithium diffusion and phase change dedicated to the single transition metal phosphate system. In our study, we measure ionic diffusivity using two methods and show how the domino-cascade model can be incorporated into the depiction of phase changes, which occur during the charge/discharge process of a dual transition metal phosphate.

Apparent diffusivity values were calculated using the relationship between peak current, linear sweep rate and diffusion constant as shown in Eq. 1 (full derivation can be found in Ref. 14).

$$\frac{i_P}{m} = 0.4463\left(\frac{F^3}{RT}\right)^{1/2} C^*_{Li} v^{1/2} A_e D^{1/2}_{app} \qquad [1]$$

where i_p is the peak current, m is the mass of the active material in the electrode, F is the Faraday constant, C^*_{Li} is the initial concentration of Li in the fully lithiated system [i.e., (bulk density of active material/molar mass) ≈ 0.0228 mol/cm^3], v is the sweep rate, A_e is the electrode area, and D is the apparent Li ion diffusion coefficient. As shown by Ref. 15 (the study through which this work was inspired), cyclic voltammetry (CV) profile peak currents are affected by the electrolyte through which the ion passes. For this reason, the calculated diffusion coefficients using this technique are apparent values that incorporate bulk Li diffusivity, Li transfer between two nanophase domains within a crystalline grain, and Li transfer through the electrolyte/solid interface.[15]

Two key assumptions need to be adopted when applying the CV based methodology previously used on a lithium single transition metal phosphate to a dual transition metal phosphate: (1) Each peak corresponds to a separate, distinct redox couple, and so (2) the effective mass for a specific redox reaction refers to only that portion of the active material contributing to the respective redox peak (i.e., $m = 0.5m_{act}$). It has become generally accepted that Li transfer occurs preferentially along [010] channels.[4,5,16,17] Assuming that the powders have a random distribution of planes (a valid assumption based on the XRD patterns in Fig. 1), the active area was taken to be one-third that of the measured Brunauer, Emmett, and Teller method (BET) surface area ($A_e = (1/3)*A_{BET}$, an approximation also suggested by Yu et al.).

Graphs of i_p/m vs $v^{1/2}$ were generated, and slopes were obtained from the linear regime of these plots. Rearranging Eq. 1 yields

$$D_{app} = \left(\frac{i_p}{mv^{1/2}}\right)^2 \frac{RT}{F^3(0.4463C^*_{Li}A_e)^2} \qquad [2]$$

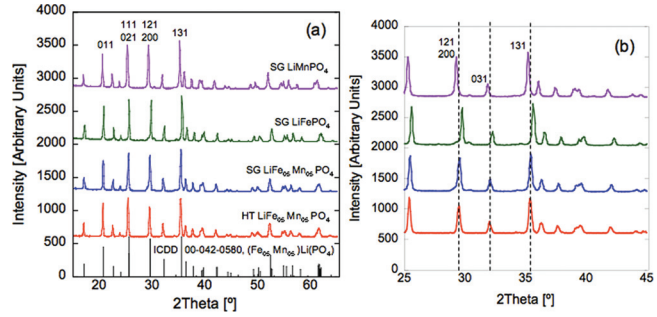

Figure 1. (Color online) (a) X-ray diffraction patterns for $LiFe_{0.5}Mn_{0.5}PO_4$ synthesized via HT and SG routes and $LiFePO_4$ and $LiMnO_4$ synthesized via the SG route; (b) magnified section of (a) showing the peak shifting associated with the addition of Mn to the transition metal site.

* Electrochemical Society Student Member.
** Electrochemical Society Active Member.
z E-mail: whitacre@andrew.cmu.edu

Downloaded on 2017-10-17 to IP 128.237.121.37 address. Redistribution subject to ECS terms of use (see ecsdl.org/site/terms_use) unless CC License in place (see abstract).

where the first fractional term corresponds to the slopes from the graph, and the second fractional term is a constant.

Because the use of CV data to interpret this system is relatively novel, a second more time consuming technique was also employed: Galvanostatic intermittent titration (GITT). Weppner and Huggins developed the following equation to relate long duration voltage transients to bulk diffusivity in ion-conducting systems[18]

$$\tilde{D} = \frac{4}{\pi\tau}\left(\frac{m_B V_M}{M_B S}\right)^2\left(\frac{\Delta E_s}{\Delta E_t}\right)^2 (\tau \ll L^2/\tilde{D})$$

where $\tilde{D}$ is the apparent chemical diffusion coefficient, L is particle size, τ is the time for which a constant current was applied, m_B is the active material mass, M_B is the atomic weight of the active material, V_M is the molar volume of the sample, S is the area of the sample/electrolyte interface, ΔE_t is the total transient voltage change of the cell for an applied galvanostatic current and ΔE_s is the change of the steady-state voltage of the cell for each step.

In this study, we examine several different $LiMPO_4$ cathode materials including $LiFe_{0.5}Mn_{0.5}PO_4$ and a composite of $LiMnPO_4$ and $LiFePO_4$. Both CV and GITT techniques were employed to determine apparent diffusivities at various degrees of lithiation and study phase transitions associated with different states of charge in this class of materials. Following is a description of this work.

Experimental

Materials synthesis.— Method A: sol–gel (SG).— Lithium acetate dihydrate, iron(II) acetate, manganese(II) acetate, and phosphoric acid were reacted in ethylene glycol in a 1:0.5:0.5:1 molar ratio to form a gel with a precursor concentration of 0.75 M. This concentration was chosen based on superior performance of $LiMPO_4$ derived from 0.75 M gels previously reported.[19] After rigorous stirring followed by a gelation period of at least 3 days, the gel was fired at 700°C in an inert environment for 12 h. To avoid oxidation, the furnace was purged with N_2 gas for 2 h before starting the heat treatment process. A thin layer of discolored material, assumed to indicate oxidation, was scraped off the top of the gel. During firing, residual amounts of carbon from the organic solvent remained on the surface of particles, providing an in situ carbon coating.

$LiFePO_4$ and $LiMnPO_4$ were fabricated in a similar way with appropriate precursor stoichiometric ratios. No discolored layer was visible on the surface of the $LiMnPO_4$ gel.

Method B: hydrothermal synthesis (HT).— $LiFe_{0.5}Mn_{0.5}PO_4$ was synthesized at Hydro Quebec and donated to Carnegie Mellon for testing. This fabrication method is discussed in detail in Ref. 20.

In all cases, active material (80 wt %) was mixed with Polyvinylidene fluoride (10 wt %) and acetylene black (10 wt %) in 1-methyl 2-pyrolidinone (NMP) into a homogeneous slurry. The slurry was subsequently deposited on a metal current collector and dried at ~110°C. Coin cells were assembled in a glovebox under an argon atmosphere using Li metal as the anode, a polypropylene separator, and a 1 M $LiPF_6$ in EC/DEC 1:2 (by volume) electrolyte (Novolyte Technologies).

Three sets of stainless steel coin cells, each loaded with less than 6 mg/cm^2 of active cathode (positive) material, were assembled: (1) SG $LiFe_{0.5}Mn_{0.5}PO_4$, (2) HT $LiFe_{0.5}Mn_{0.5}PO_4$, and (3) 50 wt % $LiFePO_4$ + 50 wt % $LiMnPO_4$. Cell (3), the composite cathode, was created for control purposes to examine the performance of Fe and Mn transition metal redox reactions, in separate crystals yet in the same cell.

Structural characterization techniques.— X-ray diffraction.— A Rigaku Geigerflex Theta-Theta x-ray diffractometer and an X'Pert Pro MPD x-ray diffractometer, each equipped with a Cu anode, were used to generate XRD patterns. All powders were tested in their fully lithiated state before any electrochemical cycling. Scans were conducted from $10° \leq 2\theta \leq 70°$ with a 0.05° step size.

Scanning electron microscopy (SEM).—Images capturing the shape and morphology of fully lithiated particles were taken with a Philips XL30 Scanning Electron Microscope at working distances less than 20 mm and at acceleration voltages varying between 10 and 20 kV. Electron dispersive spectroscopy (EDS) was used to verify sample composition. Spectra were collected at a constant working distance and acceleration voltage of 10 mm and 10 kV, respectively.

BET surface area measurements.—Specific surface areas were measured using a Quantachrome Nova 2000 surface area analyzer. The sample holder was first degassed: it was heated to 300°C for 2 h under vacuum in order to evaporate any moisture that could interfere with the surface area measurements. After cooling, the surface area measurements were conducted in a constant volume environment where nitrogen gas molecules were adsorbed onto the particle surfaces at a constant temperature (regulated with liquid N_2).

Electrochemical testing.—Electrochemical tests were all conducted at room temperature on a Bio Logic VMP3 Multi-Channel Potentiostat/Electrochemical Impedance Spectrometer. The reference and counter electrodes were both connected to the Li-foil anode, yielding a cell potential value equivalent to that of the positive electrode versus Li metal.

CV.—CVs were conducted between 2.5 and 4.5 V to ensure both Fe and Mn redox reactions could take place. All cells were tested at scan rates no higher than 0.5 mV/s.

Galvanostatic intermittent titration.—GITT was conducted using current pulses of 10 μA(25 μA for the composite cell) for 1000 s followed by a 1000 s rest periods. Potential boundaries of 2.5–4.1 V were imposed. Due to the intensity of data, calculations of ionic diffusivity values for each pulse/rest combination as described by Ref. 18 were conducted in an automated fashion, using a macro written in VISUAL BASIC FOR APPLICATIONS (VBA).

Results

Structural characterization.— XRD patterns of HT and SG materials (Fig. 1) verify the existence of single-phase crystalline $LiFe_{0.5}Mn_{0.5}PO_4$ in both cases. Peak parameters were collected using X'Pert Data Viewer software, and lattice parameters were calculated from the [011] peak, and [111]/[021] peak parameters in Wolfram MATHEMATICA 7.0. Lattice parameters for both the single solution samples differed by no more than 0.02 Å in any direction. For the SG sample, a = 6.0405 Å, b = 10.4625 Å, and c = 4.6986 Å, and for the HT sample, a = 6.0430 Å, b = 10.4688Å, and c = 4.7131 Å. These results are consistent with the literature.[9,21–23] Figure 1b is a magnified view of a section of the XRD patterns in Figs. 1a. It clearly shows the placement of $LiFe_{0.5}Mn_{0.5}PO_4$ peaks between $LiFePO_4$ and $LiMnPO_4$ peaks. For SG-$LiFePO_4$, a = 5.9968 Å, b = 10.3868 Å, c = 4.6784 Å, and for SG $LiMnPO_4$, a = 6.0898 Å, b = 10.5478 Å, c = 4.7238 Å. The higher lattice parameters for $LiMnPO_4$ were expected due to the larger atomic radius of Mn.

The SEM micrographs shown in Figs. 2 and 3 depict the similar morphologies of $LiFe_{0.5}Mn_{0.5}PO_4$ synthesized via both routes. In all

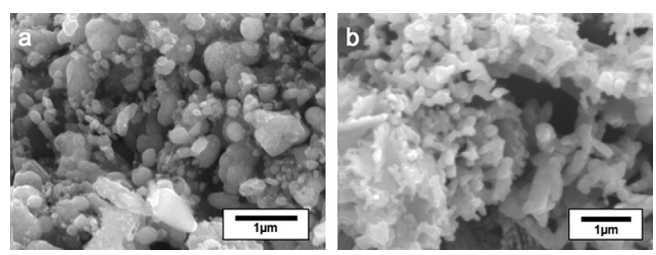

Figure 2. Secondary electron images of (a) HT-$LiFe_{0.5}Mn_{0.5}PO_4$ and (b) SG-$LiFe_{0.5}Mn_{0.5}PO_4$.

Downloaded on 2017-10-17 to IP 128.237.121.37 address. Redistribution subject to ECS terms of use (see ecsdl.org/site/terms_use) unless CC License in place (see abstract).

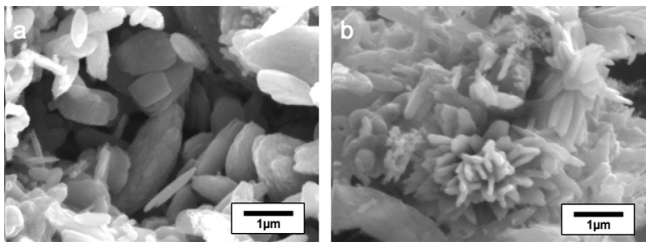

Figure 3. Secondary electron images of (a) SG-$LiFePO_4$ and SG-$LiMnPO_4$.

cases, the resulting particles were on the submicrometer scale. The needle-like shape of the $LiMnPO_4$ suggests that it should have a higher surface area than the SG-$LiFePO_4$, however, Table I indicates otherwise. The $LiFePO_4$ may be more porous, resulting in its similar specific surface area.

The data tabulated from the EDS spectra (Table II) confirm the 0.5:0.5 Fe:Mn ratio in both HT and SG $LiFe_{0.5}Mn_{0.5}PO_4$ samples.

Electrochemical characterization.— Galvanostatic discharge curves were collected for both the $LiFe_{0.5}Mn_{0.5}PO_4$ specimens at a C/78 discharge rate. Figure 4 shows the similarity in materials produced, with the HT specimen exhibiting a slightly higher specific capacity of approximately 105 mAh/g, as compared to 93 mAh/g from the SG specimen. A discharge profile is also presented for the composite cell at C/98 where there is essentially no Mn plateau, illustrating the rate limitability of the $LiMnPO_4$, and the total specific capacity was 44 mAh/g. This study is focused on examining the differences in ionic diffusivity in the dual transition metal phosphate system, as compared to the single transition metal phospho-olivine, and we understand that our specific capacities are lower than those reported for similar materials synthesized using alternate methods.

CVs collected for both SG and HT $LiFe_{0.5}Mn_{0.5}PO_4$ (Fig. 5) exhibit identical characteristics for Fe and Mn redox couples, respectively. There is a distinct potential separation between Mn anodic and cathodic current peaks, characteristic of a two-phase regime with an increased degree of irreversibility. On the other hand, the slight overlap of Fe anodic and cathodic peaks represents a "more reversible" reaction that can be associated with a single phase transition. This is consistent with recent findings published by Roberts et al.[24] where CVs were used to qualitatively describe phase transitions in the $LiFe_{1-y}Mn_yPO_4$ system. The difference in phase transition behavior between the cells containing Fe/Mn in solid solution and the composite $LiFePO_4 + LiMnPO_4$ cell is made clear by the definite separation of Fe peaks and Mn peaks (Fig. 6), expected for the cell containing two single transition metal phosphates, each of which undergoes a dual phase transition during lithiation/delithiation. The degree of separation is quantified in Fig. 7 where the Fe redox reactions in both solid solution systems exhibited lowest degrees of separation (characteristic of single phase transitions) followed by both Mn redox reactions in solid solution. As expected, both Fe and Mn redox reactions from the composite cell exhibited the highest degrees of separation, consistent with dual phase transitions.

Table I. Specific surface areas of the $LiMPO_4$ samples as calculated using the BET measurement technique.

Material	Specific surface area (m^2/g)
HT-$LiFe_{0.5}Mn_{0.5}PO_4$	37.3
SG-$LiFe_{0.5}Mn_{0.5}PO_4$	11.9
SG-$LiFePO_4$	10.5
SG-$LiMnPO_4$	12.6

Table II. Fe:Mn mass ratios collected by EDS for both HT and SG $LiFe_{0.5}Mn_{0.5}PO_4$ samples. Values given are in wt %.

	HT	SG
Fe	50.35	49.51
Mn	49.65	50.49

Raw GITT data are shown in Fig. 8 for the HT sample. Here, the Fe and Mn plateaus are approximately equal in specific capacity, in contrast to Fig. 4. The slightly higher specific capacity Mn plateau may be attributed to the limited ionic diffusivity in the Mn regime at the discharge rate used, preventing some of the Li ions associated with the Mn redox couple from being accessed at the higher rate.

GITT provides another dimension to this analysis in that it provides ionic diffusivity values at different states of charge, in comparison to the average values for Fe and Mn redox regimes provided by CV analysis. The diffusivity values in the Mn regime range from 10^{-19} to 10^{-15} cm^2/s for the HT sample, whereas the range for the same regime in the SG sample is an order of magnitude higher, spanning 10^{-18}–10^{-14} cm^2/s. In the Fe regime, the diffusivity values remain more constant, hovering approximately half an order of magnitude above and below $10^{-16}cm^2/s$ (with the exception of the last 10% of charge where values jump to as high as $10^{-13}cm^2/s$) for the HT specimen, and $10^{-14.5}$ for the SG cell.

Discussion

To our knowledge, this is the first time that CVs have been used to determine apparent diffusivity values in this mixed redox couple phospho-olivine system. A previous study by Nakamura et al.[25] reported the use of cyclic voltammetry to determine apparent diffusivity values in $LiFe_{1-x}Mn_xPO_4$ with $x < 0.2$; however, it focused solely on the effect of Mn substitution on properties of the Fe^{2+}/Fe^{3+}redox reaction. By incorporating a greater amount of Mn into the system, we examine both Fe^{2+}/Fe^{3+} and Mn^{2+}/Mn^{3+} redox reactions and suggest diffusivity values for each regime, instead of a single diffusivity value calculated using the Fe peak.

The high degree of separation (i.e., higher degree of irreversibility) between Mn anodic and cathodic peaks, as compared to the

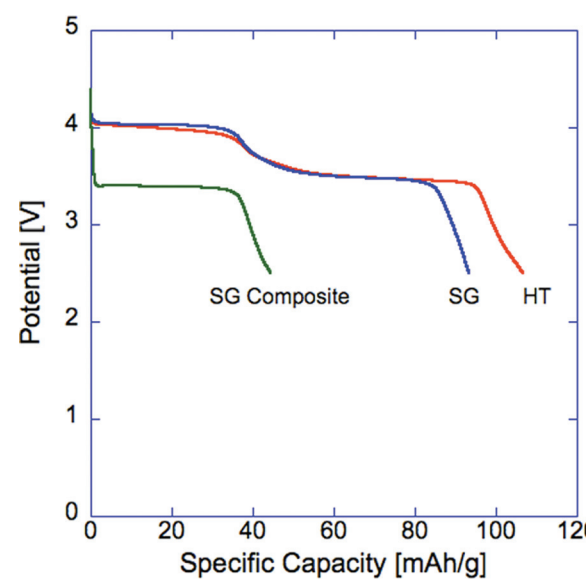

Figure 4. (Color online) Characteristic discharge curves for HT and SG $LiFe_{0.5}Mn_{0.5}PO_4$ (C/78) and SG-$LiFePO_4$+SG-$LiMnPO_4$ (C/98).

Downloaded on 2017-10-17 to IP 128.237.121.37 address. Redistribution subject to ECS terms of use (see ecsdl.org/site/terms_use) unless CC License in place (see abstract).

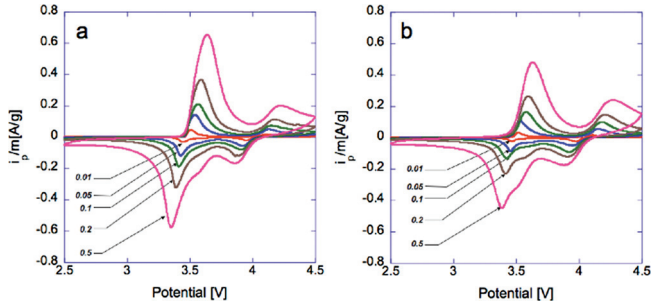

Figure 5. (Color online) Normalized cyclic voltammagrams from (a) HT $LiFe_{0.5}Mn_{0.5}PO_4$ and (b) SG $LiFeMnPO_4$. The sweep rate of each test indicated on the graphs is in millivolts per second.

degree of separation between the Fe anodic and cathodic peaks is consistent with the phase diagram of Yamada et al.[11] This diagram suggests that during delithiation of $LiFe_{0.5}Mn_{0.5}PO_4$, the Fe^{2+}/Fe^{3+} regime comprised primarily one phase and the Mn redox regime comprised two phases.

At an Fe:Mn ratio of 0.4:0.6, the notion of a single phase Fe^{2+}/Fe^{3+} redox reaction has been countered by Bramnik et al.[26] who propose two phase delithiation reactions in both Fe and Mn redox regimes of $LiFe_{0.4}Mn_{0.6}PO_4$ with the support of high resolution x-ray diffraction data. Their study suggests that an intermediate solid solution domain exists in the "region where the Fe^{2+}/Fe^{3+} electrochemical reaction is replaced by Mn^{2+}/Mn^{3+}" in the $0.55 \leq x \leq 0.67$ region of $Li_xFe_{0.4}Mn_{0.6}PO_4$. As suggested also by Roberts et al.,[24] the unusual shoulder that occurs around 3.5 V (in both the $LiFe_{0.5}Mn_{0.5}PO_4$ cells) may speak to this solid solution region, followed by the more prominent cathodic peak attributed to the remaining two phase reaction; however, this is yet to be supported by electron microscopy. Neutron diffraction may be used in the future to determine how Li site occupancy differs in the anodic and cathodic directions at various states of charge, causing the appearance of this artifact solely upon discharge.

The processed GITT data (Fig. 9) clearly depicts variable diffusivity values in the Mn regime. The linear decrease in ionic diffusivity with increased states of charge in the Mn regime is consistent with the notion of a moving phase boundary as described by the domino-cascade model as applied to the $LiFePO_4$ system.[13] This model describes the delithiation of $LiFePO_4$ in the context of subdomains of which one is depleted of lithium content before the next, causing the $FePO_4/LiFePO_4$ interface to move at different states of charge.

The domino-cascade model can be applied to dual phase regions (i.e., the Mn redox regime) in $LiFe_{0.5}Mn_{0.5}PO_4$ but cannot be used to describe what may or may not be the single phase Fe redox regime in this system. The relative consistency between apparent diffusivity values in the Fe regime suggests that it consists primarily of a single phase, which would be in agreement with the study by Yamada et al. The slight slope may be caused by the use of a constant molar volume value, which in fact is not the case at various states of charge. The shallow slope may also be indicative of a slower moving phase boundary, so that the idea of two phases cannot be entirely excluded.

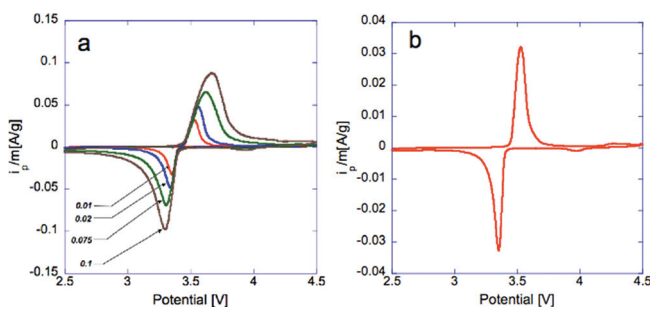

Figure 6. (Color online) (a) Normalized cyclic voltammagram from the composite cathode 0.5 $LiFePO_4 + 0.5LiMnPO_4$. The sweep rate of each test indicated on the graph is in millivolts per second. (b) An enlarged version of the CV at 0.01 mV/s is presented on the right.

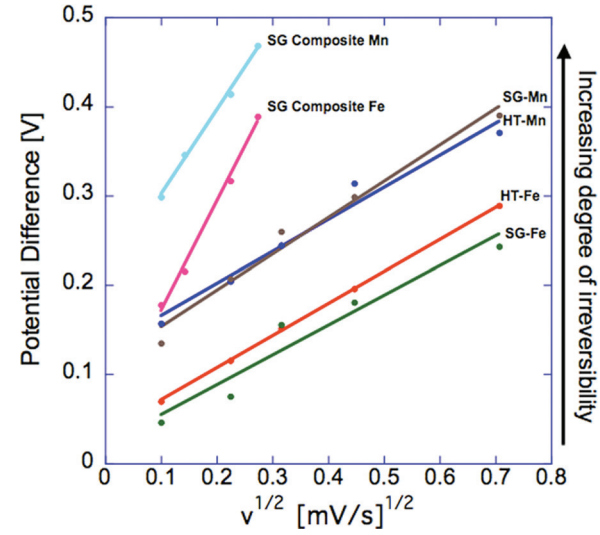

Figure 7. (Color online) Variation in potential difference between anodic and cathodic current peaks as a function of the square root of CV sweep rate.

In order to illustrate the potential one phase Fe^{2+}/Fe^{3+} region, we assume that half of the Li ions are associated with the Fe sites and the other half are associated with the Mn sites. With this, we propose the following phase transitions that occur at various stages of delithiation (Fig. 10)

(1) For ($x \leq 0.5$, single phase),
$Li_{0.5}Fe_{0.5}Li_{0.5}Mn_{0.5}PO_4 \rightarrow$
$Li_{0.5-x}Fe_{0.5}Li_{0.5}Mn_{0.5}PO_4 + xLi^+ + xe^-$

(2) For ($0.5 < x < 1.0$, dual phase),
$Fe_{0.5}Li_{0.5}Mn_{0.5}PO_4 \rightarrow$
$(1\text{-}x)Fe_{0.5}Li_{0.5}Mn_{0.5}PO_4 + xFe_{0.5}Mn_{0.5}PO_4 + xLi^+ + xe^-$

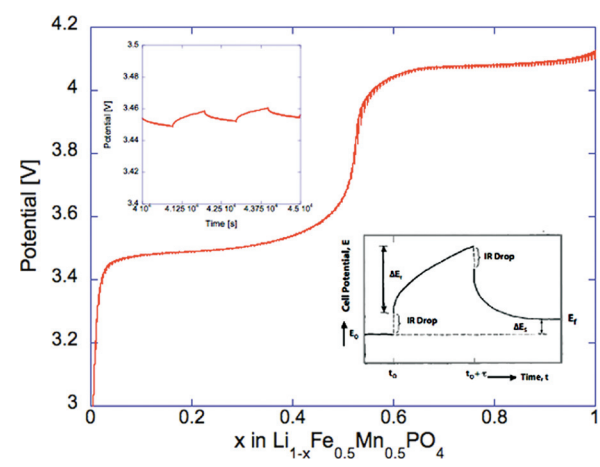

Figure 8. (Color online) GITT data for SG $LiFe_{0.5}Mn_{0.5}PO_4$. Inset top: Focused portion of raw data; bottom: schematic according to Weppner and Huggins.[18]

Downloaded on 2017-10-17 to IP 128.237.121.37 address. Redistribution subject to ECS terms of use (see ecsdl.org/site/terms_use) unless CC License in place (see abstract).

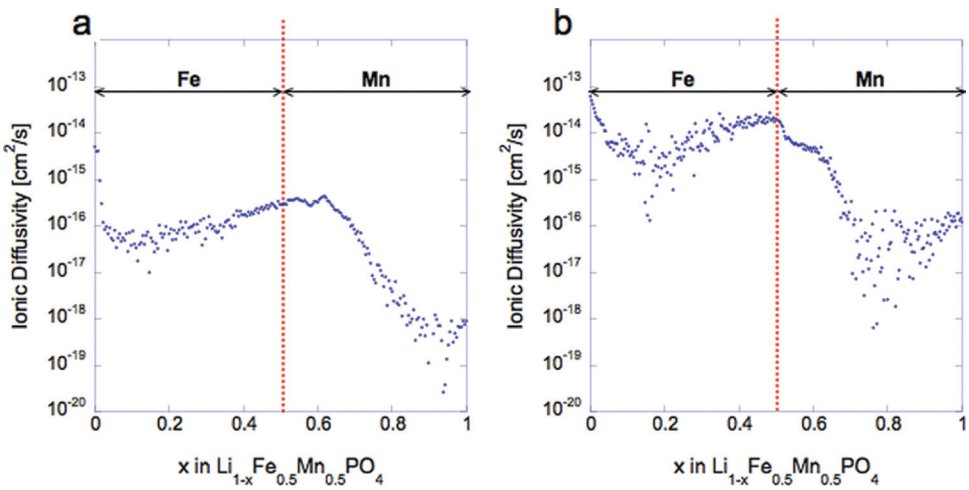

Figure 9. (Color online) Apparent diffusivity as a function of state of charge for $LiFe_{0.5}Mn_{0.5}PO_4$ as calculated from GITT data: (a) HT on the left and (b) SG on the right. The y-axis is on the logarithmic scale.

Fig. 10 illustrates the suggested phase changes that occur at various degrees of delithiation in $LiFe_{0.5}Mn_{0.5}PO_4$. Here, in the first 50% of charge, dark blue to light blue indicates the progression of $Li_{0.5}Fe_{0.5}Li_{0.5}Mn_{0.5}PO_4$ to $Fe_{0.5}Li_{0.5}Mn_{0.5}PO_4$. The uniformity of colors across the horizontal matrix from $0 \leq x \leq 0.5$ represents a single phase after which the domino-cascade model takes over ($0.5 < x < 1$), and fully delithiated nanodomains start to form.

Analysis of D values obtained from CV.— In both $LiFe_{0.5}Mn_{0.5}PO_4$ cells, lithium diffusivity in the Mn redox regime was slower than in the Fe redox regime. CVs for this system that have been published by others[1,24] have identical current peak heights for both Fe and Mn redox reactions. The lower Mn diffusivities in our samples are likely due to an intrinsic structural property attributed to the methods of synthesis. Given that the apparent diffusivity values calculated using CV and GITT data are consistent with each other in all cases (with the exception of the apparent ionic diffusivity in the Fe regime for the HT $LiFe_{0.5}Mn_{0.5}PO_4$, which will require further exploration before an explanation can be presented) (Table III), we believe that either technique can be used to successfully measure apparent diffusivity in a single or dual transition metal phosphate. A lithium diffusivity value was not calculated for the Mn regime of the composite cell due to the fact that the material was too rate limited to generate useful GITT data.

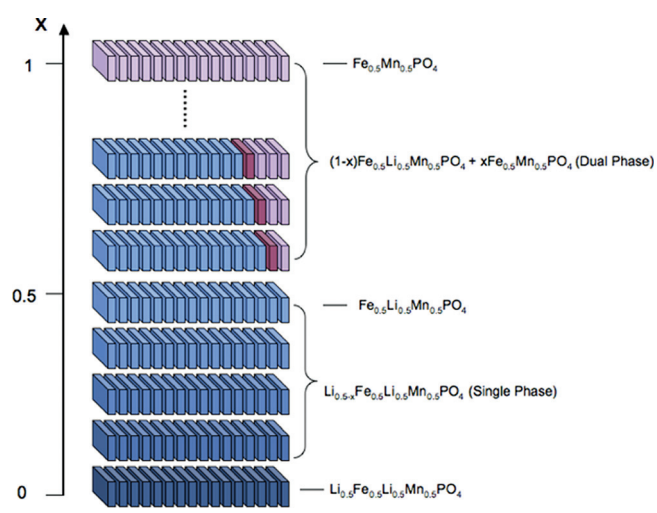

Figure 10. (Color online) Schematic representation illustrating the phase changes that occur at various degrees of delithiation in $LiFe_{0.5}Mn_{0.5}PO_4$. Here, in the first 50% of charge, dark blue to light blue indicates the progression of $Li_{0.5}Fe_{0.5}Li_{0.5}Mn_{0.5}PO_4$ to $Fe_{0.5}Li_{0.5}Mn_{0.5}PO_4$. The uniformity of colors across the horizontal matrix represents a single phase. At $x = 0.5$, the domino-cascade model according to Delmas et al.[13] takes over and fully delithiated nanodomains start to form.

The cell containing HT fabricated material had lower apparent diffusivities than the cell containing the SG synthesized specimen (Table III), despite exhibiting a higher specific capacity (Fig. 4). The lower specific capacity of the SG cell may have been limited by electronic conductivity; the in situ carbon coating offered by the ethylene glycol during heat treatment may not have offered as intimate a coating as the separate carbon coating step imposed on the HT materials.

Comparing diffusivity values obtained from the SG solid solution cell with those from the SG composite cell shows that the incorporation of Fe and Mn into the same crystalline structure resulted in improved diffusivity in the Mn redox regime. By incorporating Fe onto Mn sites of $LiMnPO_4$, the smaller Fe atoms may leave more room for the Li ions to travel, offering the observed increase in speed.

Analysis of D values obtained from GITT.— The shape of the plots of D_{app} versus degree of lithiation (Fig. 9) obtained for both HT and SG solid solution specimens is very similar; however, the most notable difference is the fact that D values obtained for the HT sample are consistently lower than those obtained for the SG cell. The discrepancy illustrates the high degree of sensitivity to synthesis parameters in the phospho-olivine system, particularly in the light that these materials are essentially indistinguishable from an XRD perspective. Variations in morphology and carbon coating, neither of which is represented by the XRD patterns, may be responsible for the differences in materials performance. Discussion on the effect of synthesis route on the performance on $LiFePO_4$ can be found in Ref. 27.

Comparison of values obtained using CVs and GITT.— The diffusivity values obtained from the CVs are within the ranges of those calculated in the respective Fe and Mn redox regimes using GITT. Averages were taken of the GITT values from 0 to 50% lithiation and 50 to 100% lithiation to make a direct comparison to the assumed average D_{Li} values, which resulted from the CV analysis. The CV values and GITT averages were in agreement with one another in the Mn regime and were within an order of magnitude in the Fe regime for both $LiFe_{0.5}Mn_{0.5}PO_4$ cells. The discrepancy between CV and GITT measured values in the Fe redox regime may

Downloaded on 2017-10-17 to IP 128.237.121.37 address. Redistribution subject to ECS terms of use (see ecsdl.org/site/terms_use) unless CC License in place (see abstract).

Table III. Calculated apparent diffusivity values from CV and GITT data. Li–Fe and Li–Mn refer to the lithium diffusion coefficients corresponding to the Fe and Mn redox reaction peaks/plateaus, respectively.

	CV		GITT	
Material	Li–Fe	Li–Mn	Li–Fe	Li–Mn
(HT) $LiFe_{0.5}Mn_{0.5}PO_4$	1.8×10^{-15}	1.6×10^{-16}	2.4×10^{-16}	1.2×10^{-16}
(SG) $LiFe_{0.5}Mn_{0.5}PO_4$	9.3×10^{-15}	2.4×10^{-15}	1.1×10^{-14}	2.0×10^{-15}
(SG) $LiFePO_4 + LiMnPO_4$	1.2×10^{-15}	1.4×10^{-17}	3.8×10^{-15}	N/A

be attributed to the fact that this redox reaction comprised both single and dual phase transitions. If the shoulder apparent in the cathodic direction is superimposed into the peak in the anodic direction, only the more prominent dual phase peak is used in the apparent diffusivity calculation, leading to a value that does not take the single phase transition into account.

Conclusions

A novel approach was taken using CVs to calculate apparent diffusivity values in this dual transition metal system, attributing half of the active material mass (i.e., half of the Li ions) to each redox reaction. Hydrothermal and sol–gel synthesis routes were used to fabricate $LiFe_{0.5}Mn_{0.5}PO_4$. Apparent diffusivity values calculated using CVs were within the upper and lower boundaries of those values calculated using GITT data. Diffusivity values in the Mn regime were consistently lower than those in the Fe regime, and the coexistence of Fe and Mn on the transition metal sites resulted in higher apparent diffusivity values with respect to Mn as compared to $LiMnPO_4$.

Interestingly, the hydrothermally synthesized $LiFe_{0.5}Mn_{0.5}PO_4$ exhibited consistently lower ionic diffusivities than that fabricated via the sol–gel route despite having a higher specific capacity.

Both CV and GITT measurement techniques exhibited signature characteristics, which confirmed the existence of a two phase Mn^{2+}/Mn^{3+} region. The overlap in Fe anodic and cathodic peaks along with the shallower slope of D_{app} versus degree of delithiation in the Fe regime leads us to believe that the reaction is predominantly a single phase one, with the existence of two phases during the final $\sim$10% of discharge.

To our knowledge, this is the first time the interpretation of phase transitions in $LiFe_{0.5}Mn_{0.5}PO_4$ has been described by the localization of half of the Li atoms with Fe and half with Mn. Our model remains consistent with the findings displayed in previous works on $LiFe_{0.5}Mn_{0.5}PO_4$ as well as the domino-cascade model by Delmas et al., which was incorporated into the interpretation of the results presented.

Acknowledgments

Thanks to Karim Zaghib of Hydro Quebec for providing hydrothermally produced samples and Carnegie Mellon University for funding this research.

Carnegie Mellon University assisted in meeting the publication costs of this article.

References

1. C. A. Burba and R. Frech, *J. Power Sources*, **172**, 870 (2007).
2. H. H. Chang, C. C. Chang, H. C. Wu, Z. Z. Guo, M. H. Yang, Y. P. Chiang, H. S. Sheu, and N. L. Wu, *J. Power Sources*, **158**, 550 (2006).
3. C. M. Burba and R. Frech, *Spectrochim. Acta, Part A*, **65**, 44 (2006).
4. M. S. Islam, D. J. Driscoll, C. A. J. Fisher, and P. R. Slater, *Chem. Mater.*, **17**, 5085 (2005).
5. C. A. J. Fisher, V. M. H. Prieto, and M. S. Islam, *Chem. Mater.*, **20**, 5907 (2008).
6. P. Jozwiak, J. E. Garbarczyk, M. Wasiucionek, I. Gorzkowska, F. Gendron, A. Mauger, and C. M. Julien, *Solid State Ionics*, **179**, 46 (2008).
7. C. M. Julien, K. Zaghib, A. Mauger, M. Massot, A. Ait-Salah, M. Selmane, and F. Gendron, *J. Appl. Phys.*, **100** (2006).
8. S. K. Martha, B. Markovsky, J. Grinblat, Y. Gofer, O. Haik, E. Zinigrad, D. Aurbach, T. Drezen, D. Wang, G. Deghenghi, et al., *J. Electrochem. Soc.*, **156**, A541 (2009).
9. A. K. Padhi, K. S. Nanjundaswamy, and J. B. Goodenough, *J. Electrochem. Soc.*, **144**, 1188 (1997).
10. A. Yamada and S. C. Chung, *J. Electrochem. Soc.*, **148**, A960 (2001).
11. A. Yamada, Y. Kudo, and K. Y. Liu, *J. Electrochem. Soc.*, **148**, A1153 (2001).
12. A. Yamada, Y. Kudo, and K. Y. Liu, *J. Electrochem. Soc.*, **148**, A747 (2001).
13. C. Delmas, M. Maccario, L. Croguennec, F. Le Cras, and F. Weill, *Nature Mater.*, **7**, 665 (2008).
14. A. J. Bard and L. R. Faulkner, *Electrochemical Methods: Fundamentals and Applications*, John Wiley & Sons, Hoboken, NJ (2001).
15. D. Y. W. Yu, C. Fietzek, W. Weydanz, K. Donoue, T. Inoue, H. Kurokawa, and S. Fujitani, *J. Electrochem. Soc.*, **154**, A253 (2007).
16. D. Morgan, A. Van der Ven, and G. Ceder, *Electrochem. Solid-State Lett.*, **7**, A30 (2004).
17. C. Y. Ouyang, S. Q. Shi, Z. X. Wang, X. J. Huang, and L. Q. Chen, *Phys. Rev. B*, **69**, 104303 (2004).
18. W. Weppner and R. A. Huggins, *J. Electrochem. Soc.*, **124**, 1569 (1977).
19. J. S. Yang and J. J. Xu, *J. Electrochem. Soc.*, **153**, A716 (2006).
20. K. Zaghib, M. Dontigny, P. Charest, J. F. Labrecque, A. Guerfi, M. Kopec, A. Mauger, F. Gendron, and C. M. Julien, *J. Power Sources*, **185**, 698 (2008).
21. T. Honma, K. Nagamine, and T. Komatsu, *Ceram. Int.*, **36**, 1137 (2010).
22. J. Molenda, W. Ojczyk, K. Swierczek, W. Zajac, F. Krok, J. Dygas, and R. S. Liu, *Solid State Ionics*, **177**, 2617 (2006).
23. J. Molenda, W. Qjczyk, and J. Marzec, *J. Power Sources*, **174**, 689 (2007).
24. M. R. Roberts, G. Vitins, G. Denuault, and J. R. Owen, *J. Electrochem. Soc.*, **157**, A381 (2010).
25. T. Nakamura, K. Sakumoto, S. Seki, Y. Kobayashi, M. Tabuchi, and Y. Yamada, *J. Electrochem. Soc.*, **154**, A1118 (2007).
26. N. N. Bramnik, K. G. Bramnik, K. Nikolowski, M. Hinterstein, C. Baehtz, and H. Ehrenberg, *Electrochem. Solid-State Lett.*, **8**, A379 (2005).
27. M. Koltypin, D. Aurbach, L. Nazar, and B. Ellis, *J. Power Sources*, **174**, 1241 (2007).

Downloaded on 2017-10-17 to IP 128.237.121.37 address. Redistribution subject to ECS terms of use (see ecsdl.org/site/terms_use) unless CC License in place (see abstract).